Cancer Letters 506 (2021) 152–166

Contents lists available at ScienceDirect

Cancer Letters

journal homepage: www.elsevier.com/locate/canlet

High-pressure oxygen rewires glucose metabolism of patient-derived glioblastoma cells and fuels inflammasome response

Chiara Arienti [a,*], Sara Pignatta [a], Michele Zanoni [a], Alice Zamagni [a], Michela Cortesi [a], Anna Sarnelli [b], Antonino Romeo [c], Donatella Arpa [c], Pasquale Longobardi [d], Daniela Bartolini [e], Luigino Tosatto [f], Antonella Naldini [g], Anna Tesei [a,**]

[a] Biosciences Laboratory, Istituto Scientifico Romagnolo per lo Studio e la Cura dei Tumori (IRST) IRCCS, Meldola, Italy
[b] Medical Physics Unit, Istituto Scientifico Romagnolo per lo Studio e la Cura dei Tumori (IRST) IRCCS, Meldola, Italy
[c] Radiotherapy Unit, Istituto Scientifico Romagnolo per lo Studio e la Cura dei Tumori (IRST) IRCCS, Meldola, Italy
[d] Hyperbaric Centre, Ravenna, Italy
[e] Pathology Unit, Bufalini Hospital, Cesena, Italy
[f] Department of Neurosurgery, Bufalini Hospital, Cesena, Italy
[g] Unit of Cellular and Molecular Physiology, Department of Molecular and Developmental Medicine, University of Siena, Siena, Italy

ARTICLE INFO

Keywords:
Glioblastoma
Hypoxia
Inflammation
Radioresistance
Preclinical studies

ABSTRACT

Human glioblastoma (GBM) is one of the most feared primary malignant brain tumors. We investigated the effect of hyperbaric oxygen (HBO) on GBM patient-derived cells and on microglia cell biology (CHME-5). HBO administered to GBM cells inhibited cell proliferation, downregulated hypoxia-inducible factor 1 α (HIF-1α) expression, and induced glucose metabolism reprogramming (glucose rewiring). It also affected the ability of a cell to perpetuate its lineage, give rise to differentiated cells and interact with its environment to maintain a balance between quiescence, proliferation and regeneration (stemness features). Such an effect may be ascribable to an increase in intracellular ROS levels and to the triggering of inflammasome signaling by HBO itself through caspase1 activation. Moreover, the results obtained from the combination of HBO and radiotherapy (RT) clearly showed a radiosensitising effect of HBO on GBM cells grown in both 2D and 3D, and a radioprotective effect of HBO in CHME-5. In addition, the exposure of M0 microglia cells to exhausted medium or extracellular vesicles (EVs) of HBO-treated GBM cells upregulated the expression of pro-inflammatory cytokines IL1β, IL6 and STAT1, whilst also downregulating the anti-inflammatory cytokine PPARγ. Collectively, these data provide a scientific rationale for the use of HBO in combination with RT for the treatment of patients with GBM.

1. Introduction

Glioblastoma (GBM) is the most aggressive brain tumor and one of the deadliest cancers, with a median overall survival of only 15 months [1]. Currently, the standard approach to manage GBM includes maximal safe surgical resection followed by external beam irradiation five times a week for six weeks, together with oral temozolomide daily [2]. Despite advances in surgery, radiation, and conventional chemotherapeutic treatments, the majority of patients relapse within 6.9 months of the initial diagnosis [3]. The poor clinical outcome of GBM is generally attributed to its intratumoral heterogeneity [4], the highly invasive nature of tumor cells, making complete surgical resection virtually impossible [5], and the presence of cancer stem cells (CSCs) [6].

One of the distinctive pathological features of grade IV glioma is the presence of necrotic foci with surrounding cellular pseudopalisades and microvascular hyperplasia, typical hallmarks of complete or partial

Abbreviations: GBM, glioblastoma; HBO, hyperbaric oxygen; HIF-1α, hypoxia-inducible factor 1 α; RT, radiotherapy; EV, extracellular vesicle; CSC, cancer stem cell; TAM, tumor-associated macrophage; ATA, atmosphere absolute; ROS, reactive oxygen species; HBOT, hyperbaric oxygen therapy; TME, tumor microenvironment.

* Corresponding author. Biosciences Laboratory, Istituto Scientifico Romagnolo per lo Studio e la Cura dei Tumori (IRST) IRCCS, Via P. Maroncelli 40, Meldola, 47014, Italy.
** Corresponding author.
E-mail addresses: chiara.arienti@irst.emr.it (C. Arienti), anna.tesei@irst.emr.it (A. Tesei).

https://doi.org/10.1016/j.canlet.2021.02.019
Received 3 September 2020; Received in revised form 19 February 2021; Accepted 22 February 2021
Available online 27 February 2021
0304-3835/© 2021 The Authors. Published by Elsevier B.V. This is an open access article under the CC BY-NC-ND license (http://creativecommons.org/licenses/by-nc-nd/4.0/).

deprivation of oxygen [7]. Hypoxia has long been associated with increased tumor aggressiveness, poor prognosis and resistance to radiotherapy and chemotherapy in different cancers, including GBM. In particular, it has been hypothesized that oxygen deprivation promotes the spread of GBM cells, favoring cell disposition at the perivascular niche and allowing escape from the adverse microenvironment [8]. The establishment of a hypoxic microenvironment also impacts immune cell composition and cell metabolism remodeling by the activation of hypoxia-sensitive factors (*e.g.* HIF 1–2) and pro-inflammatory transcription factors (*e.g.* NF-κB) [9,10]. In particular, it has been reported that hypoxia is a typical microenvironmental feature of chronically inflamed tissues [11] and, in fact, the most hypoxic areas of numerous solid tumors show a pronounced congregation of M2-like macrophages, concurring to the assessment of the immunosuppressive tumor microenvironment [12,13]. Literature data report that the function of many immune cells within and around GBM tissue tend to be severely impaired. Moreover, the immune cell component appears to be composed mainly of tumor-associated macrophages (TAMs), which may account for 30% of the total tumor mass [14]. TAMs can be peripheral myeloid cells or brain-resident microglia [15], both capable of adopting classic (proinflammatory, M1) and alternative (anti-inflammatory, prohealing, M2) activation states that impact tumor niche behavior [16]. In tumors, including GBM, the induction of hypoxia-inducible factor 1 alpha (HIF-1α) expression leads to the upregulation of the glycolysis metabolic pathway, enhancing adenosine triphosphate (ATP) production required for cell survival and proliferation [17,18]. It also increase lactate production which, in glioma cells, contributes to tumor hypoxic acidosis [19], associated with increased aggressiveness, poor prognosis and radio- and chemotherapy resistance [18].

A potential alternative therapeutic approach to reversing or partially mitigating the hypoxic immunosuppressive GBM microenvironment could hyperbaric oxygen therapy (HBOT). HBOT is based on the administration of pure oxygen (*i.e.* 100 %) to patients at pressures greater than one standard atmosphere (ATM), *i.e.* >1 atm absolute (ATA). HBOT is widely used as an additional treatment for ischemic diseases [20]. In oncology, HBOT in combination with radiotherapy (RT) is believed to act as an RT adjuvant, enhancing the amount of dissolved oxygen in the blood and peripheral tissue, and also increasing the free-reactive oxygen species (ROS), which leads to DNA damage [21]. In addition, a study on *in vivo* experimental models by Hatfield et al. [22] suggested that high oxygen concentrations may also positively impact the adenosine-rich tumor microenvironment, a typical feature of inflammation, enhancing tumor regression and long-term survival in mice. Furthermore, the results from non-randomized clinical trials conducted on Japanese GBM patients [23] suggest that RT after HBOT confers a survival benefit for patients with recurrent high-grade gliomas. However, a scientific rationale for the use of HBO in combination with radiation, base on the evaluation of the crosstalk between oxygen sensing pathways and inflammation effector cells, is still lacking.

In the present work we investigated the radiosensitising action of different HBO pressures (1.9 and 2.5 ATA) and their effect on the glycolytic metabolism of GBM and microglia cells in *in vitro* patient-derived models of GBM.

2. Materials and methods

2.1. Cell lines

Primary cultures of GBM (G34, G40 and G44) were isolated in our laboratory from surgical samples of GBM obtained from the Neurosurgery Unit of Bufalini Hospital in Cesena and selected by a pathologist. CHME-5 cell line (transformed human microglial cells) was kindly provided by Prof. Di Virgilio of the University of Ferrara. Primary cultures were maintained in NeuroCult™ for primary neuronal and neural stem cell culture (Stemcell Technologies, Vancouver, Canada) at 37 °C. CHME-5 cells were maintained in DMEM high glucose, supplemented with 10% FBS and 1% L-glutamine (Euroclone, Milan, Italy) at 37 °C. All cell lines were maintained in hypoxic conditions (4% O2).

2.2. Human specimens

Fresh tumor tissue was obtained from patients undergoing surgical resection in the Neurosurgery Unit of Bufalini Hospital (Cesena, Italy) and selected by a pathologist. The Ethics Committee of IRST and AVR (Area Vasta Romagna) reviewed and approved the study protocol (B004) and patients provided written informed consent.

2.3. Patient clinical characteristics

Samples were collected from 10 patients with GBM, 8 of whom at the first diagnosis (G40 and G44 primary cell lines were isolated from 2 of these) and 2 with recurrent disease (from whom derived G34 primary cell culture). One patient had relapsed 12 months after HBO and radiotherapy. The group consisted of 7 males and 3 females aged 40–80 years, median age 62 years (Table S1).

2.4. In vitro radiation system

The flasks containing monolayer cells or 3D-spheroids were inserted into a custom-built plexiglass phantom (40 × 40 × 8 cm). The phantom was irradiated using a 6-MV photon beam delivered by an Elekta Synergy linear accelerator (Elekta Oncology Systems, Stockholm, Sweden). The delivered dose was calculated using the Philips Pinnacle 3 radiation therapy planning system (Philips Healthcare, Best, The Netherlands) customized with the geometric and dosimetric characteristics of an Elekta Synergy linear accelerator, as previously described [24].

2.5. Treatments

HBOT was performed in a hyperbaric chamber designed expressly for preclinical studies. The air inside the chamber was replaced with 100% O_2 and the pressure increased for 15 min until 1.9 and 2.5 ATA (absolute atmospheres) were reached. The latter conditions were maintained for 1 h. Finally, decompression from 2.5 to 1.9 ATA back to atmospheric pressure was done gradually over 15 min.

Radiation. Within 30 min of HBOT, cells were irradiated in 25-cm^2 flasks or 96-multiwell plates using the linear acceleration Elekta Synergy Platform system. The doses delivered were 5 Gy and 7.5 Gy.

2.6. In vitro cytotoxicity assay

3D cell viability was measured using the CellTiter-Glo® 3D Cell Viability Assay (Promega, Milan, Italy) 72 h after the treatments. Spheroids were removed from the 96-well low-attachment culture plates and placed separately in single wells of a 96-well opaque culture plate (BD Falcon, Corning, Somerville, MA, USA). CellTiter-Glo® 3D reagent was added to each well and the luminescence signal was read after 30 min using the GloMax® bioluminescent reader (Promega).

2.7. Soft agar colony formation assay

Soft agar colony formation assay was performed as described by Borowicz et al. [25]. After two weeks' incubation, the resulting colonies were counted: colonies with >50 cells were quantified under inverted microscope (I500X, Olympus, Tokyo, Japan) by two independent observers. The count was repeated each week up to a maximum of 5 weeks' incubation.

2.8. In vitro glucose uptake activity

Glucose uptake assay was performed with Glucose Uptake-Glo™

Assay according to the manufacturer's instructions (Promega). Briefly, cells exposed to different radiation doses (5 and 7.5 Gy) and oxygen pressures (1.9 and 2.5 bars) were washed with PBS-1X and incubated with 2-deoxy-D-glucose (2DG) for 10 min. After several additions of buffer, the uptake of 2DG was measured according to the manufacturer's instructions and luminescence intensity (Relative light unit, RLU) was recorded using a GloMax® Luminometer (Promega).

2.9. In vitro lactate activity

Lactate assay was performed with Lactate-Glo™ Assay (Promega) according to the manufacturer's protocol. Briefly, cells exposed to different radiation doses (5 and 7.5 Gy) and oxygen pressures (1.9 and 2.5 bars) were incubated with lactate detection reagent for 60 min at a 1:1 ratio of cell medium and lactate detection solution. The luminescence signal was recorded using a GloMax® Luminometer.

2.10. ROS detection

The H2O2 assay was performed with ROS-Glo™ H2O2 Assay (Promega). Cells exposed to different radiation doses (5 and 7.5 Gy) and oxygen pressures (1.9 and 2.5 bars) were seeded onto an opaque white 96-well plate in the desired medium or PBS. The H2O2 substrate solution was then added, bringing the final volume to 100 μL. The plate was incubated at 37 °C in a 5% CO2 incubator for 60 min. 100 μL of the ROS-Glo detection solution was added to each well at the end of incubation. After an additional incubation of 20 min at room temperature, luminescence was recorded using a GloMax® Luminometer.

2.11. Caspase-1 activity assay

Caspase-1 activity was anlayzed with the Caspase-Glo 1 inflammasome assay kit (Promega) according to the manufacturer's protocol. Prior to the assay, the caspase-1 luminescent substrate solution was prepared and equilibrated to room temperature. After the respective incubation periods, 100 μL of the substrate solution was added to each well of the 96-well plate. The plate was then shake for 30 s and incubated at room temperature for 1.5 h to allow the luminescent signal to stabilize. The plate was then read using a GloMax® Luminometer.

2.12. NAD/NADH and NADP/NADPH detection

NAD/NADH and NADP/NADPH assays were performed with NAD/NADH-Glo™ Assay and NADP/NADPH Glo™ Assay (Promega, Milan, Italy) according to manufacturer's protocols. Briefly, cells untreated and exposed to different oxygen pressures (1.9 and 2.5 bar), were incubated with NAD/NADH or NADP/NADPH Detection Reagent for 30 min, with a 1:1 ratio of cells medium + PBS and detection solution. The luminescence signal was recorded using a GloMax® Luminometer.

2.13. LDH-Glo™ Cytotoxicity Assay

LDH release was measured in the culture supernatants with the LDH-Glo™ Cytotoxicity Assay (Promega), according to manufacturer's instructions. Briefly, 250 × 10 GBM cells were plated in a six-well plates. After HBO treatments, cell supernatants diluted 1:25 in LDH storage buffer (200 mM Tris-HCl (pH 7.3), 10% Glycerol, 1% BSA in deionized water) were added to LDH detection reagent at ratio 1:1 and incubated at room temperature for 60 min. Luminescence were then measured using the GloMax® bioluminescent reader (Promega). LDH release (%), was calculated by using the following formula: LDH release (%) = [(experimental LDH release value) − (background value)]/[(LDH release value in 10% Triton X-100-treated samples) − (background value)] × 100.

2.14. Annexin V assay

Treated and untreated cells were washed in PBS 1X and then incubated with 25 μL of Annexin V-FITC in binding buffer (Thermo Fisher Scientific, Waltham, MA, USA) for 15 min at 37 °C in a humidified atmosphere in the dark. Immediatly before flow cytometric analysis, 5 μg/mL of propidium iodide was added to discriminate between apoptotic and necrotic cells.

2.15. Western blot analysis

Briefly, cell proteins were extracted with M-PER Mammalian Protein Extraction Reagent (Thermo Fisher Scientific, Waltham, MA, USA) supplemented with Halt Protease Phosphatase Inhibitor Cocktail (Thermo Fisher Scientific). Mini-PROTEATGX™ precast gels (4–20% and any kD) (Bio-Rad Laboratories Hercules, CA, USA) were run using Mini-PROTEAN Tetra electrophoresis cells and then electroblotted by Trans-BlotTurbo™ Mini PVDF Transfer Packs (Bio-Rad Laboratories). The unoccupied membrane sites were blocked with T-TBS 1X (Tween 0.1%) and 5% non-fat dry milk to prevent nonspecific binding of antibodies and probed with specific primary antibodies overnight at 4 °C. This was followed by incubation with the respective secondary antibodies. The antibody-antigen complexes were detected by chemiluminescence with Clarity™ Western ECL Substrate (Bio-Rad Laboratories).

2.16. Comet assay

The assay was performed according to the manufacturer's protocol (Comet assay, Trevigen, Gaithersburg, MD, USA). Briefly, at the end of the treatments, 5×10^5 cells were suspended in LM Agarose (at 37 °C) at a ratio of 1:10 (v/v), and 75 μL were immediately transferred onto the comet slide. The slides were immersed for 1 h at 4 °C in a lysis solution, washed in the dark for 1 h at 4 °C in alkaline solution and then electrophoresed for 30 min at 20 V. Slides were immersed twice in dH2O for 5 min each, dipped in 70% ethanol and stained with 20 μL of diluted SYBR® Green Master Mix (Bio-Rad Laboratories). The extent of DNA damage was evaluated quantitatively by EVOS Cell Imaging Systems 10x (Thermo Fisher Scientific). The percentage of DNA in tail for different categories of comets was expressed, as previously described by Garcia et al. [26]. We used CometAnalyser tool to obtain reproducible and reliable quantitative data, as previously decribed by Pignatta et al. [27].

2.17. Confocal microscopy analysis

After HBOT, cells were fixed and permeabilized with ice-cold methanol for 10 min and acetone for 1 min on ice, blocked for 1 h at room temperature with blocking solution (1X PBS/5% normal goat serum/0.3% Triton X-100) and incubated overnight at 4 °C with primary anti-ASC antibody (1:250 dilution, Santa Cruz, Santa Cruz, USA). After washing 5 times with PBS 1X, slides were incubated for 1 h at room temperature with secondary goat anti-mouse Alexa Fluor 546 (1:250; Life Technologies, Carlsbad, CA, USA). Slides were then washed 5 times with PBS 1X and mounted. The confocal imaging was performed with a Nikon A1 confocal laser scanning microscope (Tokyo, Japan), equipped with a 60X oil objective (1.4 NA), using 405 and 561 nm laser lines.

2.18. Characterization and isolation of extracellular vesicles (EVs)

Briefly, cell lines were grown to 70% confluence, at which point the growth medium was replaced with FBS-depleted equivalent medium and exposed to HBOT. After 72 h, 200 mL of conditioned supernatant were collected and centrifuged at 500 g for 5 min at 4 °C to pellet cellular contaminant, followed by 3000 g for 30 min at 4 °C to pellet cell debris. The supernatant was centrifuged at 18,000 g for 30 min and subsequently for 30 min at 10,000 g. The resulting supernatant was

ultra-centrifuged twice at 100,000 g for 70 min and 120 min at 4 °C. The final EV pellet was solubilized in 100 μL of filter-sterilized PBS. EVs were used immediately or stored at −80 °C.

2.19. Nanoparticle tracking analysis (NTA) of EVs

Nanoparticle tracking analysis was used to determine particle size and concentration of all samples. Purified EVs were diluted in 0.22 μM of filtered PBS to an appropriate concentration before analysis, loaded into the sample chamber of a NanoSight LM10 instrument (Malvern Panalytical, Salisbury, UK). At least three videos of 30 or 60 s in length were recorded for each sample. The temperature was kept constant throughout the measurements. Data analysis was performed with NTA 3.1 software. Data is presented as the average and standard deviation of the three video recordings. When samples contained large numbers of particles, they were diluted before analysis and the relative concentration was then calculated according to the dilution factor.

2.20. Microglial polarization

CHME-5 human microglial cells were activated by a 24-h incubation with 150 nM of phorbol 12-myristate 13-acetate followed by a 24-h incubation in DMEM high medium. Microglial cells were polarized in M1 by incubation with 20 ng/mL of interferon-γ (IFN-γ). M2 polarization was obtained by incubation of the cells with 40 ng/mL of interleukin 4 and 40 ng/mL of interleukin 13. M0-like cells were exposed to untreated HBOT-exposed GBM cell medium or exosomes. Finally, microglial cells were exposed to EVs or culture medium isolated from GBM cells exposed to HBOT. Gene expression levels of M1/M2 polarization-associated markers were analyzed in CHME-5 cells exposed to each of the above conditions.

2.21. Co-culture

CHME-5 human microglial cells were activated by a 24-h incubation with 150 nM of phorbol 12-myristate 13-acetate followed by a 24-h incubation in DMEM high medium. GBM cells were pipetted into the inner circle of the underside of cell culture inserts membrane of a 0.3 μm (BD FALCON). The plate was covered with a lid, thus holding the cell suspension to the underside of the membrane by capillary action. The cells were allowed to adhere overnight at 37 °C and 5% CO2. Subsequently, the insert was placed in the well of a 24 well plate with CHME-5 M0 cells. Co-cultures were maintained for 2 days at 37 °C and then treated with HBO.

2.22. Three-dimensional cell culture

A rotatory cell culture system (RCCS) (Synthecon Inc., Houston, TX, USA) was used, as previously described [24]. The rotator bases were placed inside a humidified 37 °C incubator and connected to power supplies set up externally. Single cell suspensions of about 1×10^6 cells/mL of lung cell line were placed in the 10-mL rotating chamber at an initial speed of 12 rpm. The culture medium was changed every 4 days and tumor spheroids with an equivalent diameter ranging from about 500 to 700 μm (depending on the cell line used) were obtained in around 15 days. The spheroids were transferred into 96-well low-attachment culture plates (Corning Inc., Corning, NY, USA).

2.23. Real-time quantitative polymerase chain reaction (RT-qPCR)

Total RNA was extracted from cell lines using TRIzol® reagent following the manufacturer's instructions (Invitrogen, Carlsbad, CA, USA). Reverse transcription (RT) reactions were performed in a 20-μL volume containing 400 ng of total RNA using an iScript TM cDNA Synthesis kit (Bio-Rad Laboratories). mRNA levels of the selected genes were assessed by RT-qPCR using custom TaqMan probes (Applied Biosystems, Carlsbad, CA, USA). Gene expression was normalized with two endogenous reference genes, GAPDH and HPRT, identified as the most stable genes by the geNorm VBA applet for Microsoft Excel. Relative quantification of target gene expression was calculated using the comparative Ct method. All experiments were conducted in triplicate.

2.24. Nanostring

Total RNA was extracted from frozen tumor tissue using Qiagen DNA/RNA all prep (Qiagen, Hilden, Germany) according to the manufacturer's instructions, and hybridized with nCounter® PanCancer IO 360™ Panel (NanoString Technologies, USA). RNA concentration was evaluated using the Nanodrop 2000 spectrophotometer (NanoDrop Technologies, Wilmington, DE, USA) and quantified using Qbit. RNA quality and integrity were confirmed on Bioanalyzer Nano RNA Chip (Agilent Technologies, Santa Clara, USA). The differential mRNA expression of 770 genes (750 immune genes and 20 housekeeping genes) was quantified using the nCounter Digital Analyzer. Quality control, normalization and data analysis of count numbers were carried out with NanoString nSolver® Analysis Software v3.0 based on the geometric mean of positive controls, background thresholding, and housekeeping genes.

2.25. Statistical analysis

All experiments were performed at least three times. Quantifiable data were derived from three independent experiments. Data are reported as mean and standard deviations. The statistical analysis was carried out using GRAPH PAD PRISM 8 software or applying the Student *t*-test for 2-group comparisons or statistical one-way ANOVA as appropriate. Differences were considered statistically significant when $p \leq 0.05$.

3. Results

3.1. HBO modulates the expression of stemness-related genes in patient-derived GBM cells

In our experiments we used a panel of three GBM patient-derived primary cultures characterized by different morphology, growth rates and stemness-related phenotypes (Fig. 1A–D), thus representative of the high heterogeneity and plasticity of GBM. G34 was obtained from a patient with recurrent GBM, while G40 and G44 were obtained from naive patients who underwent a first surgical resection but who were not treated with radiotherapy and/or chemotherapy (Table S1). Notably, G34 cells showed the highest growth rate and expressed the stemness markers CD133, CD44 and Eph2a at the highest level with respect to G40 and G44 cells (Fig. 1 B, C). We exposed our primary GBM cell cultures to different HBO pressures (1.9 and 2.5 ATA) commonly used in hyperbaric medicine for clinic care of wounds [28], to investigate the HBO impact on the stemness-related expression signature. Among the stemness-related surface markers investigated we observed a significant decrease in CD44, Nestin and Slug after the exposure to 2.5 and 1.9 ATA in all cell lines tested ($0.01 < p < 0.001$; Fig. 1 D; Fig. S1). In particular, 1 h-exposure to HBO at 2.5 ATA causes the down regulation of the highest number of stemness-related markers, independently from the cell line ($p < 0.5p < 0.001$; Fig.1 D; Fig. S1).

These data highlighted the high plasticity of glioma stem cell phenotype and the capability of HBO to lead GBM cells to a non-stem phenotypic shift.

3.2. HBO causes remodeling of glucose metabolism in glioma cells and long-lasting inhibition of cell proliferation

Hypoxic stimulus has been reported to induce GLUT1 expression in a

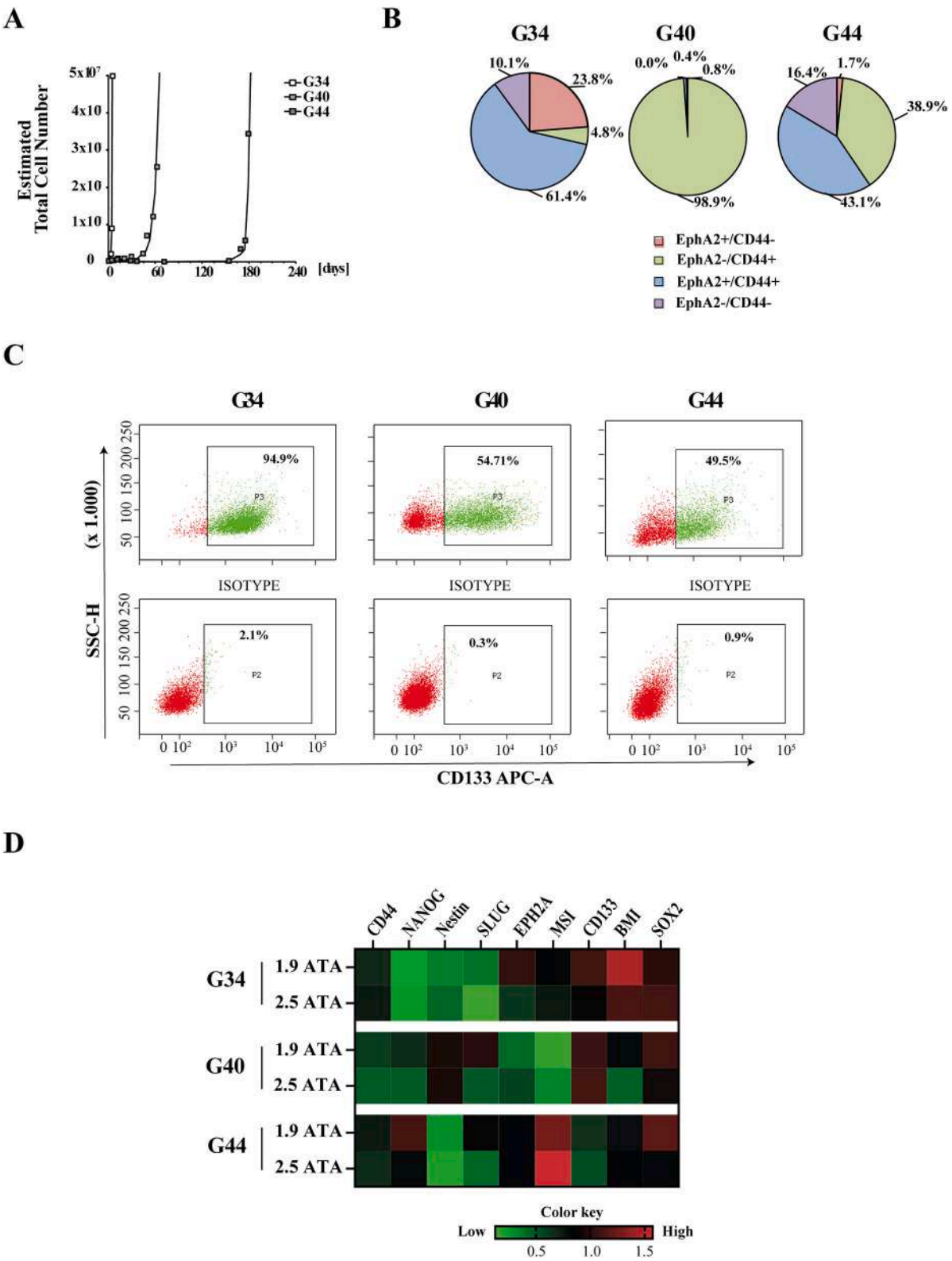

Fig. 1. Stemness-related phenotype of GBM primary cultures shaped by hyperbaric oxygen. A) GBM cell lines from 3 patients showing variable growth rates. For the analysis, all primary cultures were seeded at the same cell density (250,000 cells/plate). The cell count was plotted on the y-axis, the days on the x-axis. **B)** Expression analysis of ephrin-A and CD44 and their co-expression in human GBM cells. Cell suspensions were labeled with PE-conjugated anti-ephrin A and FITC-conjugated anti-CD44 antibodies, and analyzed by flow cytometry. **C)** Representative flow cytometry dot plot graphs showing the percentage of CD133 expression in GBM primary cultures. Isotypic controls were used to establish correct gating. **D)** Heatmaps displaying stemness-related expression patterns for GBM patient-derived primary cultures exposed to different HBO pressures. Increasing values are converted into color intensities of green and red. Each row represents a sample, and each column a gene.

HIF-1-dependent manner, leading to an increase in cellular glucose uptake and lactate production [29]. In our model, glioma cells were maintained in hypoxia (4% oxygen) before their exposure to HBO in hyperbaric chamber. A 1-h-exposure to HBO at 2.5 ATA caused a decrease of HIF-1α protein expression in all GBM primary cell cultures tested, whereas 1.9 ATA HBO exposure induced a similar effect only in G34 cells (Fig. 2A). The decrease of HIF-1α expression exerted by HBO was further confirmed by RT-qPCR analysis of mRNA expression (Fig. 2B). Moreover, in all glioma cells, as expected HBO exposure significantly reduced GLUT1 expression level ($0.05 < p < 0.001$, Fig. 2 B, Fig. S2A) concurrently with a decrease in glucose uptake ($0.05 < p < 0.001$, Fig. 2 B, Fig. S2B) and lactate production ($0.05 < p < 0.001$, Fig 2B,Fig. S2C). The remodeling of glucose metabolism exerted by HBO was paired with a significant increase in DNA damage in all glioma cells investigated, as shown by the results of the comet assay analysis (Fig. 2C). In particular, independently of the oxygen pressure used, HBO caused a significant induction of DNA damage ($p < 0.001$) in G40 cells with respect to untreated cells. A significant increase in damaged nuclei (~30%) was induced in G44 cells by 1.9 ATA HBO, whereas G34 cell nuclei were damaged by 2.5 HBO treatments ($p < 0.01$). Furthermore, HBO exposure fostered the impairment of the replicative properties of glioma cells, as shown in short- and long-term growth assays performed after 14 and 50 days in the hyperbaric chamber (Fig. 2D). Notably, the effect of 1.9 ATA HBO on proliferation was particularly evident in G44 cells where, 50 days after exposure, a >50% reduction in cell survival was observed. Moreover, when the same cell line was exposed to 2.5 HBO, a ~10% reduction in plating efficiency was observed. Exposure of G34 cells to both HBO treatments led to a significant inhibition of cell proliferation. Finally, the proliferation properties of G40 cells were also significantly compromised by HBO treatments, albeit to a lesser degree than the other two glioma cell lines. Variations observed between cell lines in response to HBO stimuli could be ascribed to their different

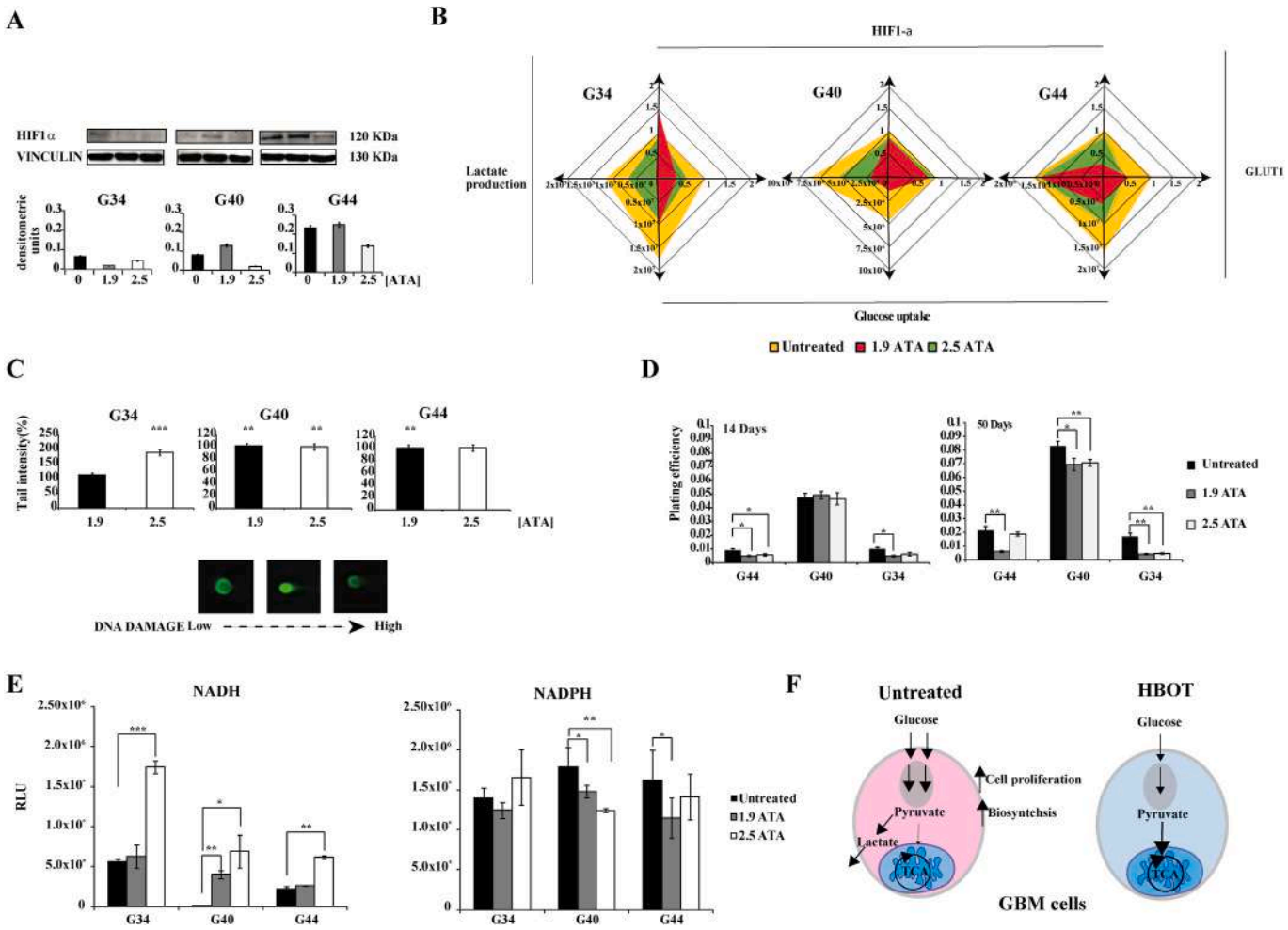

Fig. 2. Effect of HBO exposure on cellular metabolism, DNA repair proficiency and cell growth of glioma cells. A) HIF1α protein expression determined by Western blotting analysis in G34, G40 and G44 cell lines. **B) Radar chart of functional metabolic assays.** Glut1 and HIF1α mRNA expression in GBM cells was analyzed by RT-qPCR 72 h after HBOT. Graphs are representative of two independent experiments, each performed in triplicate and normalized for HPRT and GAPDH housekeeping expression. Glucose uptake and lactate production of GBM cells were measured by luminescence-based assay 24 h after exposure of HBO, as described in Materials and Methods. **C) Quantification of single and double strand breaks by comet assay**. The DNA damage was measured by alkaline comet assay. Representative photomicrographs of comet assay showing GBM cell lines stained with sybr green after HBO exposure, 10x magnification. DNA damage is expressed as a percentage of tail intensity relative to untreated cells. **D) Analysis of cell proliferation.** Survival percentage and plating efficiency were evaluated in GBM cell lines after HBOT. **E) Functional metabolic assays.** NADH and NADPH levels in GBM cells 24 h after HBOT were measured with luminescent assay. **F)** Model depicting how HBOT may induce metabolism reprogramming. In GBM cells glucose uptake increases, enhancing glycolysis. A substantial part of glucose is used into biosynthetic pathways to support cell proliferation. Pyruvate is mainly used for lactate production. Oxidative phosphorylation occurs, but it is independent from glycolysis increase. The GBM cells after HBOT convert glucose to pyruvate via glycolysis, and the pyruvate produced mainly participates in mitochondrial oxidative processes for efficient ATP production. The amount of glucose carbon flux is indicated by the relative thickness of black arrows. TCA: tricarboxylic acid cycle. Data are reported as mean ± SD for three experiments. Statistical significance was determined by Student's t-test. (*$p < 0.05$, **$p < 0$ .01, ***$p < 0.001$.

phenotype, mirroring the high heterogeneity of GBM. To further our understanding of the relationship between HBO and the rewiring of glucose metabolism, we measured NADH and NADPH levels in our cell lines after exposure to 1.9 and 2.5 ATA. An increase in NADH, especially significant after 2.5 ATA, was observed in all GBM cells ($0.05 < p < 0.001$, Fig. 2E). Conversely, the production of NADPH was decreased or unchanged with respect to that of untreated cells (Fig. 2E). These data would seem to indicate a rewiring of glucose metabolism towards mitochondrial respiration (Fig. 2F).

3.3. HBO induces NLRP3 inflammasome activation signaling

We next used confocal microscopy to analyze inflammasome formation in glioma cells after HBO. As shown in Fig. 3A, the increase of ROS was independent from partial oxygen pressures used ($0.01 < p < 0.001$).

As expected, after NLRP3 inflammasome activation we detected also a significant induction of ASC production in all cell lines following exposure to both oxygen pressures (Fig. 3 B).

Furthermore, a significant induction of caspase-1 activity was observed in G40 and G44 cell lines exposed to 1.9 and 2.5 oxygen pressures with respect to untreated cells. In particular, the activity increased to 40% in G40 cells after exposure to 2.5 HBO and to 50% in G44 line after the exposure to 1.9 HBO (Fig. 3C). Moreover, as a consequence of caspase −1 activation we observed an induction of cleaved Gasdermin D (GSDM D) in G40 cell lines exposed to 1.9 and 2.5 (Fig. 3 D). Interestingly, the HBOT also induced apoptosis activation in all cell lines in proportion to LDH release, indicating the triggering of the pyroptosis pathway (Fig. 3 E, F). These results are consistent with the significant increase in LDH release observed in all treated cells with respect to the untreated one ($p < 0.05$) (Fig. 3E). Additionally, the highest percentage of apoptotic cells was observed after 2.5 ATA (Fig. 3F).

3.4. Radiosensitising effect of hyperbaric oxygen in GBM cell lines

GBM cells exposed to 2.5 and 1.9 HBO were treated with two different radiation doses (5 Gy and 7.5 Gy) within 30 min of HBOT. Exposure to 1.9 HBO followed by radiation induced a strong growth inhibition in G44, G40 and G34 cell lines with respect to HBO treatment or radiation alone ($0.05 < p < 0.001$) (Fig. 4 A). We also detected a significant inhibition of cell viability after exposure to 2.5 HBO followed by both radiation doses in G44 and G40 cell lines ($0.01 < p < 0.001$), but not in G34 cells. Next, we focused our attention on the last glioma cell line, representative of recurrent GBM, a clinical condition for which there is still no standard of care. Exposure of G34 cells to 2.5 and 1.9 ATA HBO followed by radiation treatment induced a significant reduction in survival fraction and increase in DNA damage ($0.05 < p < 0.001$) (Fig. 4B and C). Moreover, this treatment schedule induced a remodeling of glucose metabolism with a significant reduction in glucose uptake ($0.05 < p < 0.001$) compared to irradiation alone (Fig. 4D). Furthermore, a significant increase in ROS production ($0.01 < p < 0.001$) (Fig. 4D) and caspase-1 activation ($0.05 < p < 0.001$) were observed after HBO-RT, showing a synergistic effect of the treatments in activating the inflammasome pathway (Fig. 4E). In particular, 2.5 HBO followed by 5 Gy and 7.5 Gy RT induced a 60%–80% increase in caspase-1 activity with respect to radiation alone ($0.05 < p < 0.01$).

These results were confirmed in GBM cells grown as three-dimensional (3D) cultures, which closely resemble the cytoarchitecture of clinical tumors. We observed that exposure of the 3D GBM model to HBO significantly inhibited tumor cell proliferation (Fig. 5A, $p < 0.05$) and increased DNA damage (Fig. 5B, $p < 0.05$). In particular, the combined treatment resulted in a significant induction of DNA damage, as shown by the 40% increase in DNA in the comet tail. The exposure of GBM spheroids to HBO also fostered the reprogramming of glucose metabolism, as highlighted by the decrease in glucose transporter GLUT1 expression followed by increased glucose uptake and reduced lactate production (Fig. 5C-D-E). Following HBO exposure and consequent NLRP3 inflammasome activation, ROS levels increased and caspase-1 activation was also observed (Fig. 5F and G). Finally, the exposure of G34 spheroids to HBO-RT highlighted the radiosensitising effect of HBO, confirmed by the results of the clonogenic assay and by the DNA damage observed ($p < 0.001$) (Fig. 5H and I).

3.5. HBO exerts a radioprotective effect on human microglia cell line (CHME-5) and switch off inflammasome signaling

We exposed a CHME-5 cell line grown under hypoxic conditions (4% oxygen) to the same oxygen pressures used for previous experiments. No effect was found in terms of inhibition of colony formation, DNA damage, inflammasome activation or cellular metabolism (Fig. S3 A-D). Notably, exposure to 1.9 HBO produced a slight but significant increase in survival and a decrease in the percentage of comet tail DNA intensity. Conversely, exposure to 1.9 and 2.5 HBO followed by 5 Gy or 7.5 Gy induced a significant decrease in cytotoxicity with respect to that observed after RT used alone ($p < 0.001$)(Fig. 6A). Moreover, after exposure to HBO-RT, a significant decrease in terms of DNA damage was also detected by the comet assay with respect to exposure to 5 Gy or 7.5 Gy used alone ($0.05 < p < 0.001$) (Fig. 6B). The clonogenic assay (Fig. 6C) revealed a significant increase in plating efficiency after exposure to 1.9 or 2.5 HBO followed by 5 Gy or 7.5 Gy radiation doses with respect to that observed after RT alone ($0.05 < p < 0.001$).

We also investigated the impact of HBO on the inflammasome pathway (Fig. 6 D). After 2.5 HBO followed by 7.5 Gy, caspase-1 activity significantly decreased to 60%–80% with respect to RT alone ($p < 0.01$). As expected, the same response was also obtained after exposure to 1.9 HBO followed by 5 Gy or 7.5Gy, compared to RT alone ($p < 0.05$). We also examined mRNA expression levels of proinflammatory cytokines IL-1β and IL-6 (Fig. 6E), observing a significant reduction in IL-1β expression after exposure to both oxygen pressures ($0.05 < p < 0.01$), and significantly lower IL-6 levels only after treatment with 1.9 HBO ($p < 0.05$). In addition, expression levels of both cytokines significantly decreased after exposure to 1.9 or 2.5 ATA HBO followed by 5 Gy or 7.5 Gy compared to RT alone ($0.05 < p < 0.01$).

3.6. HBO affect the crosstalk between GBM and immune microenvironment by modifying microglia polarization towards the M1-phenotype

We exposed CHME-5 M0 cells to the exhausted medium of glioma cells treated or not with HBO (Fig. 7A and B), observing a phenotypic shift towards M2-like polarization (Fig. S4A). Conversely, the expression of pro-inflammatory cytokines IL1β, IL6, STAT1 and PPARα transcription factor were highly induced in microglial cells exposed to exhausted medium of HBO-treated GBM cell (Fig. 7 B, Fig. S4B; $0.05 < p < 0.01$). In particular, M1-associated genes STAT1 was significantly expressed, while the mRNA level of the anti-inflammatory and immunosuppressive marker, PPARγ and TGF-b respectively, were consistently lower in M0 exposed to medium obtained from HBO-treated cells than in M0 cells exposed to untreated cell medium (Fig. 7 B, Fig. S4($0.05 < p < 0.001$). We explored the hypothesis that the polarization message may be conveyed by exosomes by exposing microglial cells to EVs secreted from glioma cells treated or not with HBO (Fig. 7A, C). The results showed that HBO GBM EVs, independently of the glioma cell of origin, significantly induced the expression of pro-inflammatory cytokines and M1-associated genes (Fig. 7C, Fig. S4C; $0.05 < p < 0.001$).

Then, to confirm the role of HBOT in rendering microglia less immunosuppressive, we treat co-cultures of GBM and CHME-5 M0 cells with 1.9 and 2.5 ATA. We found that the expression of pro-inflammatory cytokines IL1β, IL6, STAT1 and PPARα transcription factor were highly induced in CHME-5 M0 (Fig.7 D, Fig. S4; $0.05 < p < 0.001$). Conversely, the mRNA level of PPARγ and TGF-b were significantly lower in treated

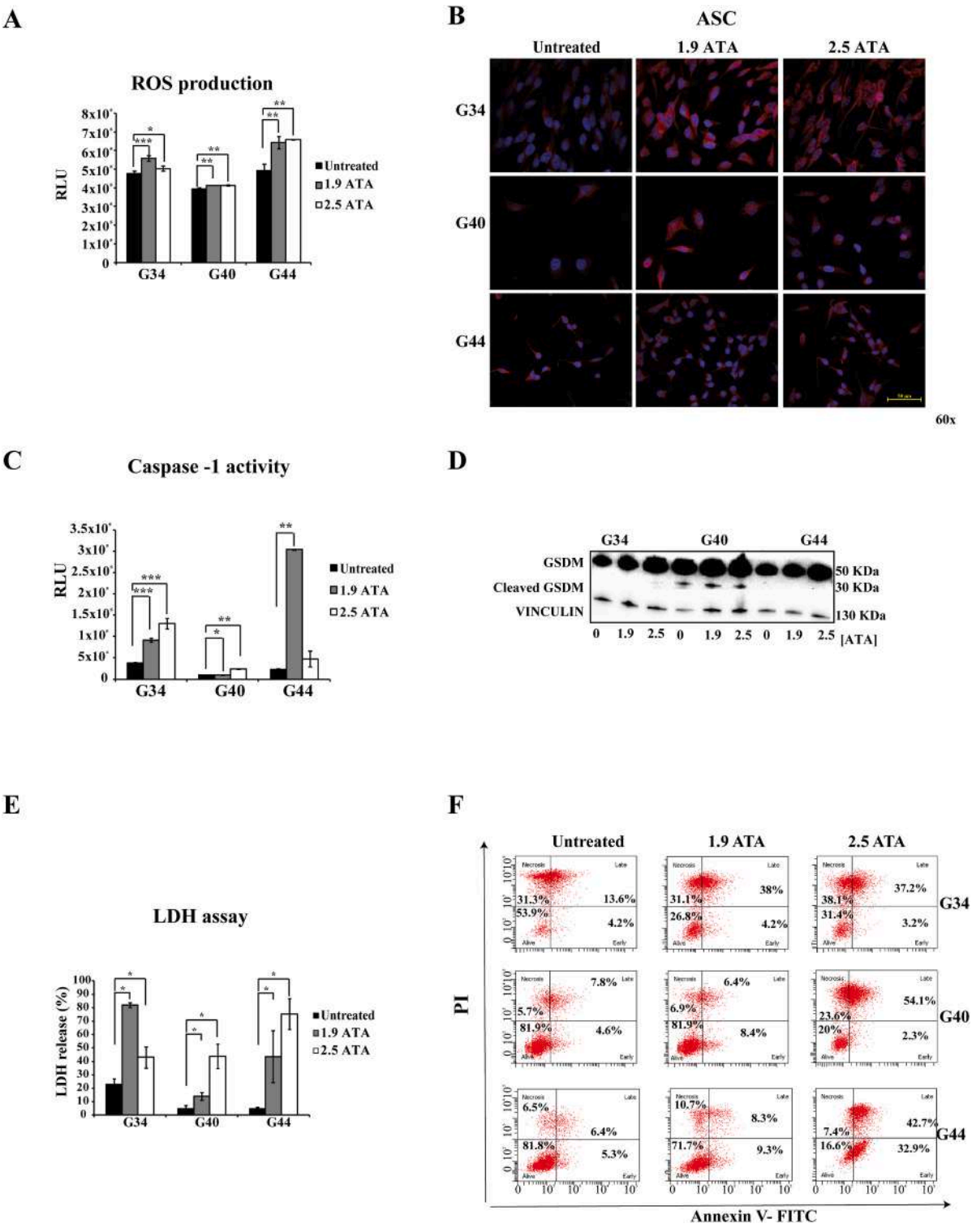

Fig. 3. Caspase-1 activation by HBOT. A) Functional metabolic assays. ROS production in GBM cells 24 h after HBOT was measured by luminescence-based assay, as described in Materials and Methods. **B)** Immunofluorescence staining with ASC antibody. The images are representative of G34, G40 or G44 cells exposed to different hyperbaric oxygen doses (1.9 and 2.5 ATA). Fluorescent DAPI staining was used to visualize nuclear DNA. Cell images were captured by Nikon Eclipse Ti2 confocal microscope with 60x plan apochromatic oil immersion objective lens. Scale bars, 50 μm. **C)** Functional metabolic assays by Caspase-Glo® 1 Inflammasome Assay in GBM cells 24 h after HBOT was measured by luminescence-based assay. **D)** Gasdermin D and cleaved GSDM D protein expressions determined by Western blotting analysis in G34, G40 and G44 cell lines. E) Functional metabolic assays. LDH release in GBM cells 24 h after HBOT (LDH-Glo™ Cytotoxicity Assay). F) Apoptosis was analyzed by Annexin V assay in G34, G40 and G44 cells 7 days after HBOT (1.9 or 2.5 ATA). Data are reported as mean ± SD for three experiments. Statistical significance was determined by Student's t-test (*$p < 0.05$, **$p < 0$ .01, ***$p < 0.001$).

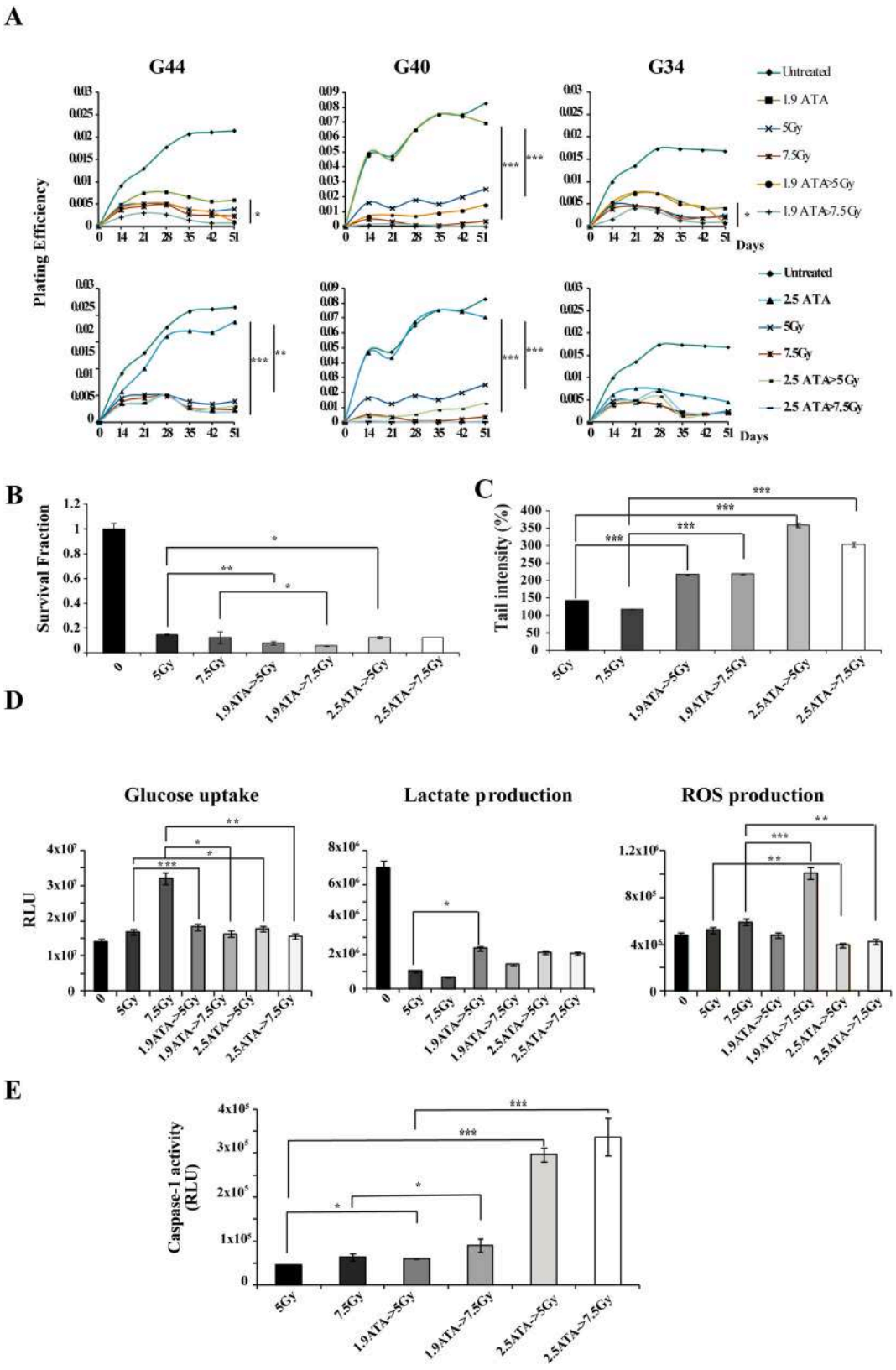

Fig. 4. Radiosensitising effect of HBOT in glioma cells. A) Cytotoxic effect evaluated as plating efficiency after RT or HBOT alone and after HBOT-RT in GBM cells. **B)** The survival fraction of G34 cells was evaluated after RT alone and after the HBOT-RT combination. Data are reported as mean ± SD. **C)** DNA damage measured in G34 cells by alkaline comet assay. DNA damage is expressed as a percentage of tail intensity relative to untreated cells. Error bars represent mean ± SE. **D)** Glucose uptake, lactate production and ROS production by G34 cells was measured by luminescence assay after RT alone and after HBOT-RT. Error bars represent mean ± SE. **E)** Evaluation of caspase-1 activity in G34 cells by Caspase-Glo® 1 Inflammasome Assay 24 h after RT alone and after HBOT-RT. Statistical significance was determined by Student's t-test (*$p < 0.05$, **$p < 0.01$, ***$p < 0.001$).

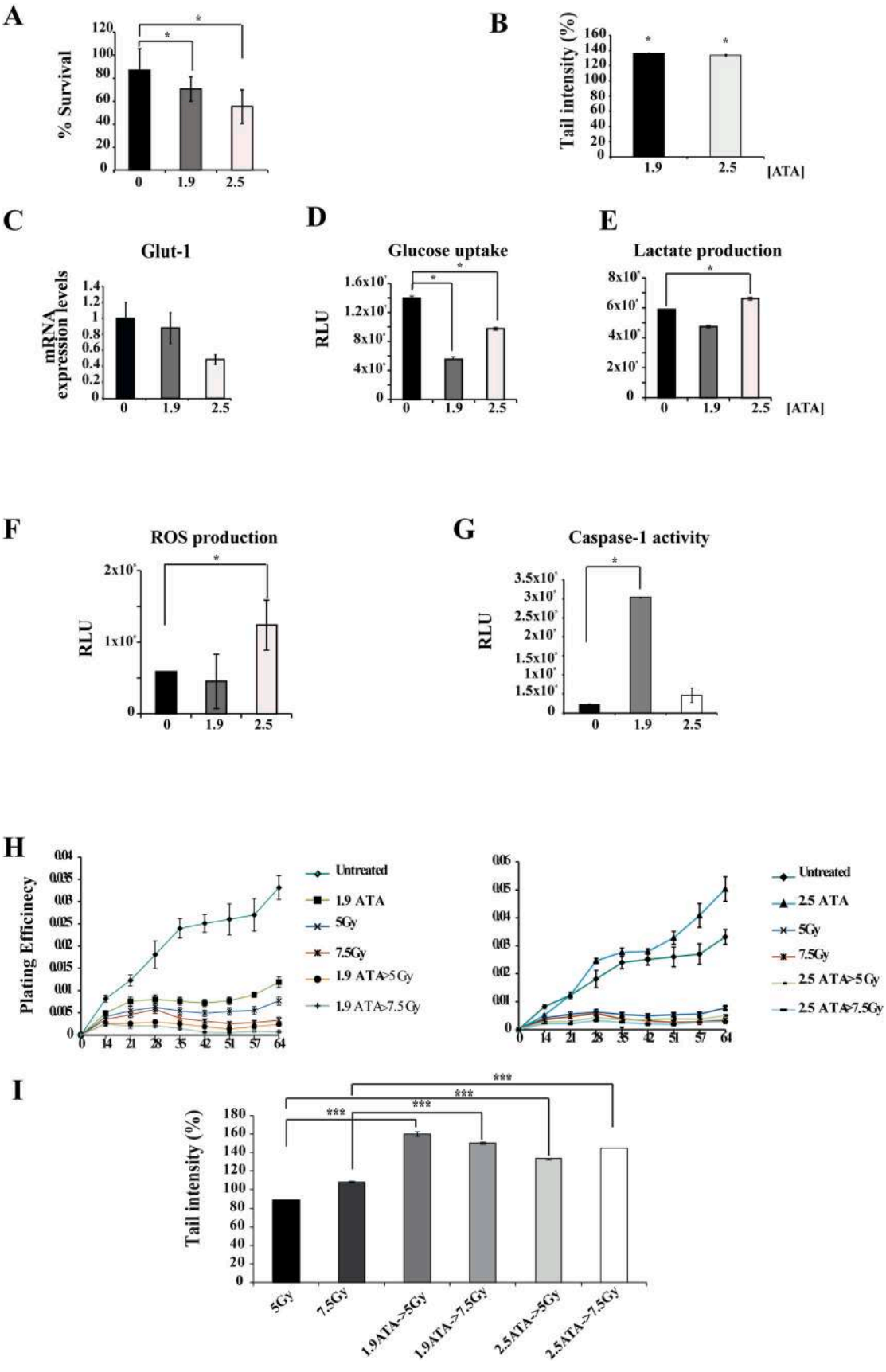

(caption on next page)

Fig. 5. Effect of HBO and HBOT-RT on *in vitro* GBM 3D model.
A) The viability of G44 spheroids was evaluated by CellTiter-Glo® 3D Cell Viability Assay 72 h after HBOT. Data are reported as mean ± SD of 3 independent experiments. **B)** DNA damage measured by alkaline comet assay in G44 spheroids. DNA damage is expressed as a percentage of tail intensity relative to untreated cells. Error bars represent mean ± SE. **C)** Glut1 mRNA was isolated in G44 spheroids 72 h after HBOT and gene expression was determined using RT qPCR. Graphs are representative of two independent experiments, each performed in triplicate. **D-E)**. Glucose uptake and lactate production by G44 spheroids was measured by luminescence assay 24 h after HBOT. **F)** ROS production in G44 spheroids was measured by luminescence assay 24 h after HBOT. Error bars represent mean ± SD. **G)** Caspase-1 activity was analyzed in G44 spheroids by the luminescent assay Caspase-Glo® 1 Inflammasome Assay 24 h after HBO. **H)** The cytotoxic effect on G44 spheroids was reported as plating efficiency after exposure to RT alone and after HBOT-RT. **I)** DNA damage measured by alkaline comet assay. DNA damage expressed as a percentage of tail intensity relative to untreated cells 72 h after RT alone and after HBOT-RT. Statistical significance was determined by Student's t-test. (*$p < 0.05$, **$p < 0$ .01, ***$p < 0.001$).

cells respect to untreated ($0.05 < p < 0.001$).

3.7. The anti-tumor effect of HBO-RT treatment schedule was showed by transcriptional profiling analysis of GBM tissues

Currently a clinical trial is ongoing at our Institute aimed to evaluate the role of HBO as radiotherapy adjuvant in the treatment of GBM recurrent patients (clinical trial N. 1851 approved by Local Committee of December 13, 2017). In the present work, we performed Nanostring transcriptional profiling analysis on 8 tissue samples obtained by naive GBM patients who underwent the first surgical removal and two samples from a GBM recurrent patient (Table S 1). One of the latter underwent surgical removal after HBO-RT treatment schedule (1-h exposure to 2.5 HBO followed by accelerated hyperfractionated radiotherapy- 25 Gy/5 fractions/5 days). Due to restricted sample size, we limited the analysis to a qualitative comparison of gene expression profile using Nanostring nCounter platform (Fig. 8A–C). As highlighted by the differential hierarchical clustering specific transcriptional signatures associated to autophagy and cell proliferation pathways were observed. In particular, down-regulation of genes involved in cell proliferation, and up-regulation of genes related to autophagy, were observed (Fig. 8A and B). Additionally, we analyzed immunoprofiling signaling, observing high expression of pro-inflammatory cytokines IL1β and IL18, and a downregulation of IL6 and TGFb in relapsed GBM patients (sample test) (Fig. 8C). These preliminary data further support the use of HBO as radiotherapy adjuvant in patients with GBM.

4. Discussion

The few preclinical studies focusing on the therapeutic use of HBOT in GBM have reported inconclusive and often contrasting results. For example, an *in vivo* study by Sthur et al. [30] demonstrated that HBOT helps to reduce GBM growth and enhance apoptosis, whereas Zang et al. reported that HBO exerts a pro-tumorigenic effect, promoting glioma cell proliferation and angiogenesis, and inhibiting apoptosis and cell cycle arrest [31]. Conversely, several clinical trials conducted mainly on Asian patients supported the use of HBOT as a radiotherapy adjuvant but did not propose a scientific rationale to back up their hypothesis [23,31,32[33]]. There may be several reasons for the discrepancies between preclinical and clinical data, not least the fact that the preclinical GBM models used to test the efficacy of HBOT were not always representative of real-life clinical conditions.

In the present work, we used a panel of GBM patient-derived low-passage primary cell cultures grown under hypoxic conditions. The cells were characterized by stemness features representative of glioma stem cells (GSCs) localized in heterogeneous cell hypoxic niches and responsible for the aggressiveness and plasticity of clinical GBM. In our model, HBO inhibited glioma cell proliferation independently of the partial oxygen pressure used. Such an effect can be ascribed to an increase in intracellular ROS levels caused by HBOT and consequently to greater DNA damage, both of which were detected in our glioma cells. However, the hampered glioma cell growth may also have been due to the triggering of inflammasome signaling by HBOT followed by the induction of pyroptosis, a form of necrotic and inflammatory programmed cell death induced by inflammatory caspase-1 [34,35]. This finding was further confirmed by the high cell death and LDH release induced by HBOT. This effect of HBOT on glioma cells has never been reported.

Furthermore, in our model we explored the hypothesis of the presence of high levels of oxygen coupled with specific oxygen tension to effectively counteract the hypoxic glioma stem cell niche [8] by reprogramming the gene expression profile and metabolism of glioma cells. We found that HBO downregulates the expression of hypoxia-inducible factor 1 (HIF-1), one of the master regulators orchestrating cellular responses to hypoxia, including the makeup of their stem cell phenotype [8]. Our experiments showed that the exposure of glioma cells to high oxygen concentrations affected their stemness features, leading them towards a non-stem phenotype. In particular, after HBOT, GBM primary cultures showed a significant reduction in expression levels of CD133 and Nestin, two stemness markers associated with tumor invasiveness and angiogenesis [35,36].

It has been established that tumor cells have an elevated rate of glucose uptake and high lactate production in the presence of oxygen, a phenomenon known as aerobic glycolysis (also called the Warburg effect) [37–39]. In our model, we observed a reprogramming of glucose metabolism with a decrease in the expression of glucose transporter GLUT1 and a reduction in glucose uptake and lactate production in all the glioma cells investigated. This is especially important because high lactate production has been reported to be capable of remodeling the tumor microenvironment (TME), contributing to acidosis which acts as a cancer cell metabolic fuel and induces immunosuppression. This leads to aggressive tumor cell proliferation, invasion, migration and resistance to treatment, including radiotherapy [40]. We also observed a strong production of NADH when GBM cell lines were exposed to HBOT that seems to indicate an increase of oxygen consumption through mitochondrial respiration.

In our *in vitro* model, HBOT prior to radiotherapy enhanced radiotoxicity in the radioresistant cell line G34. To further investigate this finding, we verified and confirmed the efficacy of the combination HBOT-RT in *in vitro* 3D GBM spheroids, which closely reproduce the spatial organization and microenvironmental elements of *in vivo* microtumors such as nutrient gradients and oxygen [40–42]. Moreover, preliminary data on the transcriptional profiling of GBM tissue by nanostring technique revealed a downregulation in cell proliferation pathways and upregulation genes linked to autophagy pathways and pro-inflammatory cytokines of in recurrent GBM patients. These findings, albeit inconclusive, indicates the importance of further investigation for the usefulness of HBOT-RT in clinical practice. Finally, we explored the impact of HBOT on the immunosuppressive microenvironment of the GCS niche, composed mainly of tumor-infiltrating microglia and macrophage populations that represent up to 50% of GBM resident non-neoplastic cells [14]. These immune tumor-infiltrating subpopulations are thought to be involved in the development of gliomas, promoting cell proliferation, angiogenesis, immunosuppression, and to contribute to chemotherapy and radiotherapy resistance [43]. We exposed the human microglia cell line CHME-5, grown under hypoxic conditions (4% oxygen), to the same treatment schedules used for the experiments on glioma cells, observing no colony formation inhibition, DNA damage or alteration in cellular metabolism after HBOT alone, thus supporting the hypothesis that hyperbaric oxygen therapy exerts a radioprotective effect on immune cells.

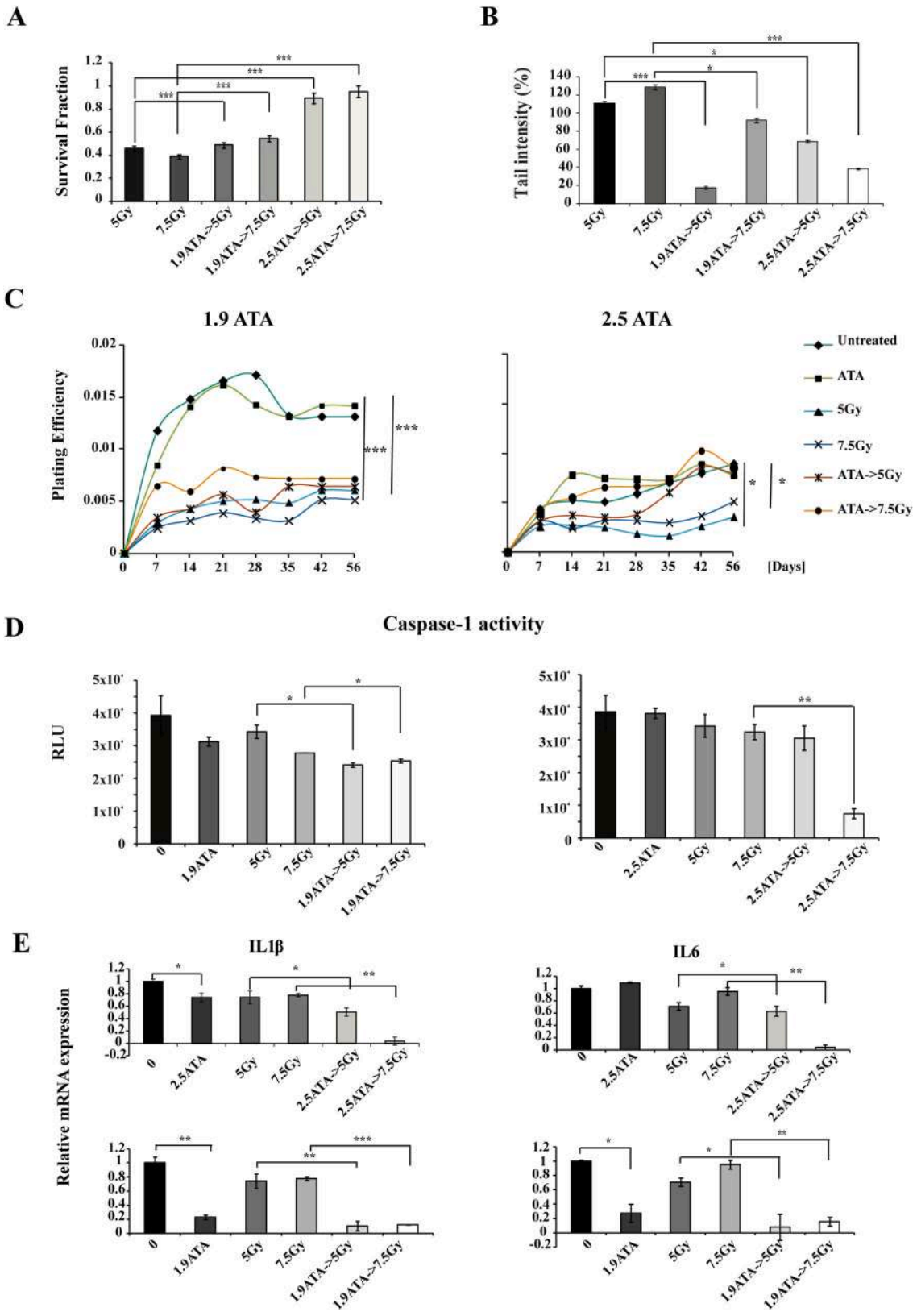

Fig. 6. Radioprotective effect of HBOT in human microglia cell line (CHME-5). A) survival fraction of CHME-5 cells was evaluated by clonogenic assay after exposure to RT alone and after HBOT-RT. Data are reported as mean ± SD of three experiments. **B)** DNA damage measured by alkaline comet assay. DNA damage was expressed as a percentage of tail intensity relative to untreated cells. Error bars represent mean ± SE of three experiments. **C)** The cytotoxic effect exerted by RT alone and by HBOT-RT in CHME-5 cell line was reported as plating efficiency. **D)** Caspase-1 activity in CHME-5 was measured by luminescence assay 24 h after HBOT or RT. **E)** mRNA expression in CHME-5 was determined by RT qPCR 4 h after HBOT or RT. Graphs are representative of two independent experiments, each performed in triplicate. Error bars represent ±SD of triplicate values. Statistical significance was determined by Student's t-test (*$p < 0.05$; **$p < 0.001$; ***$p < 0.001$).

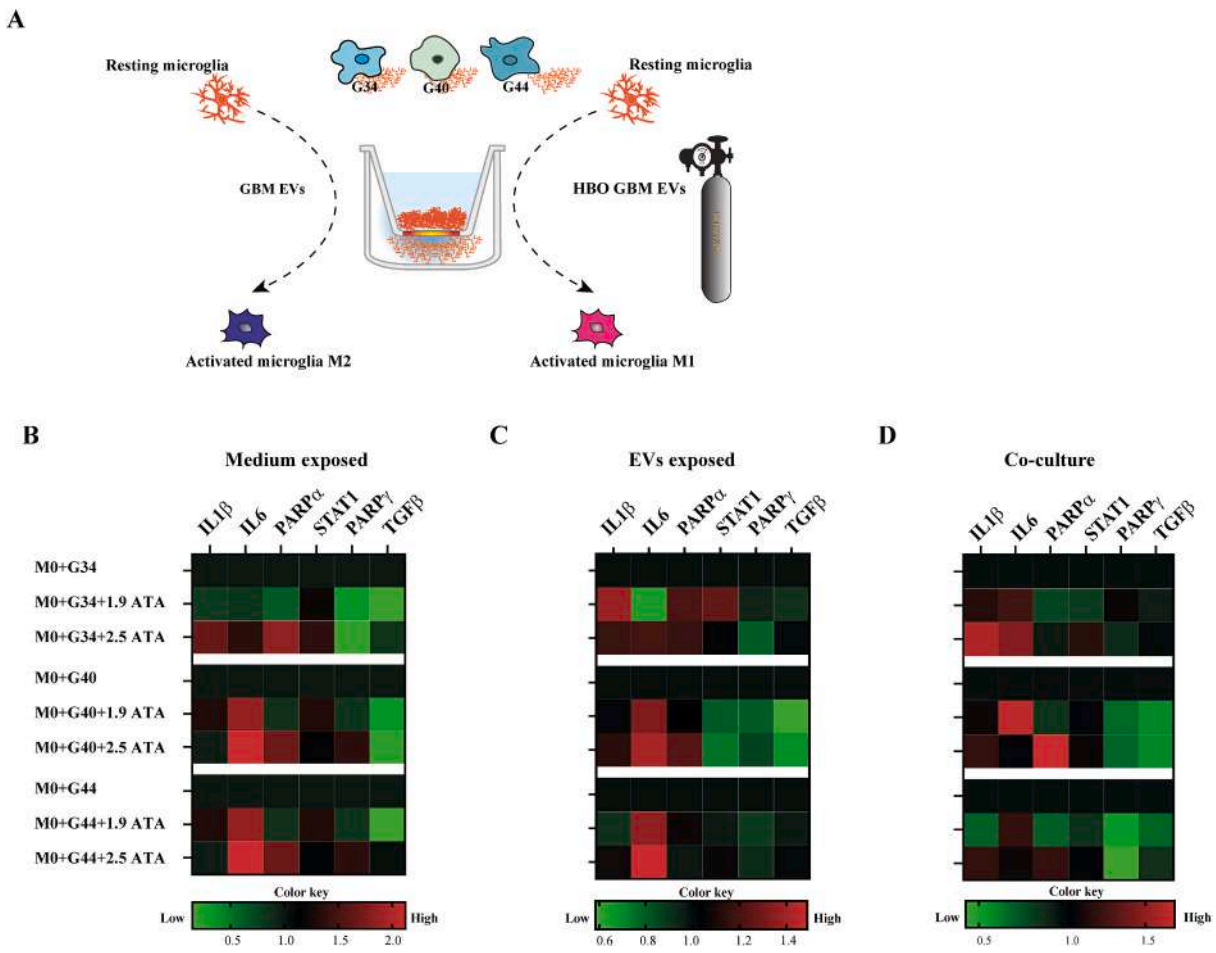

Fig. 7. A) Schematic representation of the experimental design showing G34, G40 and G44 medium or EVs obtained from untreated and HBO treated cells and administered to CHME-5 M0 cells. **B–C)** mRNA of CHME-5 M0 was isolated 72 h after exposure to G34, G40 and G44 medium or to EVs and gene expression was determined using RT-qPCR. D) mRNA of CHME-5 M0 co-cultured with G34, G40 and G44, was isolated 72 h after HBOT and gene expression was determined using RT-qPCR. Heatmap of 9 samples in a subset of expression signatures. Each row represents a sample, and each column, a gene. Red and green colors indicate the level of up- and downregulation, respectively. Graphs are representative of two independent experiments, each performed in triplicate.

It is known that microglia cells have a very efficient DNA damage response machinery and are sensitive to ROS [44]. We hypothesize that pretreatment with HBO may serve to prime the DNA damage repair capacity of microglial cells, equipping them to deal with the increase in ROS production after radiotherapy and to repair consequent DNA damage. These data were further confirmed by our findings that hyperbaric oxygen in combination with RT reduced the activation of inflammasome in the human microglia cell line by attenuating expression levels of IL-1β and IL-6. Similar results were obtained by Qian et al. who suggested that HBO alleviates the inflammatory response in traumatic brain injury by modulating microglial inflammasome signaling [45].

We also described, for the first time, the effect of HBOT on the polarization status of microglia and on the crosstalk between glioma cells and microglia. In particular, we observed that the presence of glioma cells in an *in vitro* co-culture system polarized microglia cells towards an M2-like phenotype. Conversely, exposure of M0 microglial cells grown in co-culture to HBOT upregulated the expression of several pro-inflammatory cytokines closely linked to an M1-like phenotype, such as IL1β, IL6, STAT1 and the transcription factor PPARα, whilst also downregulating the anti-inflammatory cytokines PPARγ and TGFb linked to an M2-like phenotype. Finally, we demonstrated that the polarization message was conveyed by EVs secreted by HBO-treated glioma cells, concluding that it could be a potentially important diagnostic tool for monitoring response to treatment. The literature data regarding IL6 and IL1b are controversial probably due to their frequently co-expression in both M1/M2 gene signatures [46,47]. However, there are several papers that include them in the signature of M1 like TAMs [48,49]. Our data provide evidence of the extreme plasticity that characterizes glioma cells and which can also be considered an Achilles' heel on which to base new therapeutic approaches in an effort to combat this most feared brain tumor.

In conclusion, the data obtained in our study suggest a potential use of HBO before radiotherapy as second-line treatment of patients with recurrent GBM, for whom there is still no standard of care. In particular, we showed that HBO is capable of counteracting the hypoxic GSC niche and for this reason should be considered as a potential therapeutic option for the treatment of GBM.

Author statement

Chiara Arienti: Conceptualization, Validation, Investigation, Writing-original draft, Review and Editing, Visualization. **Anna Tesei**: Supervision, conceptualization, writing-original draft, project administration, writing-Review and Editing, funding acquisition, validation. **Michela Cortesi**: investigation, Review and Editing. **Sara Pignatta**: investigation, Data Curation. **Anna Sarnelli**: Investigation. **Antonino Romeo:** Resources. **Donatella Arpa**: Methodology. **Alice Zamagni**: Investigation. **Michele Zanoni**: Investigation. **Pasquale Longobardi:** Resources, visualization. **Luigino Tosatto:** Resources. **Daniela**

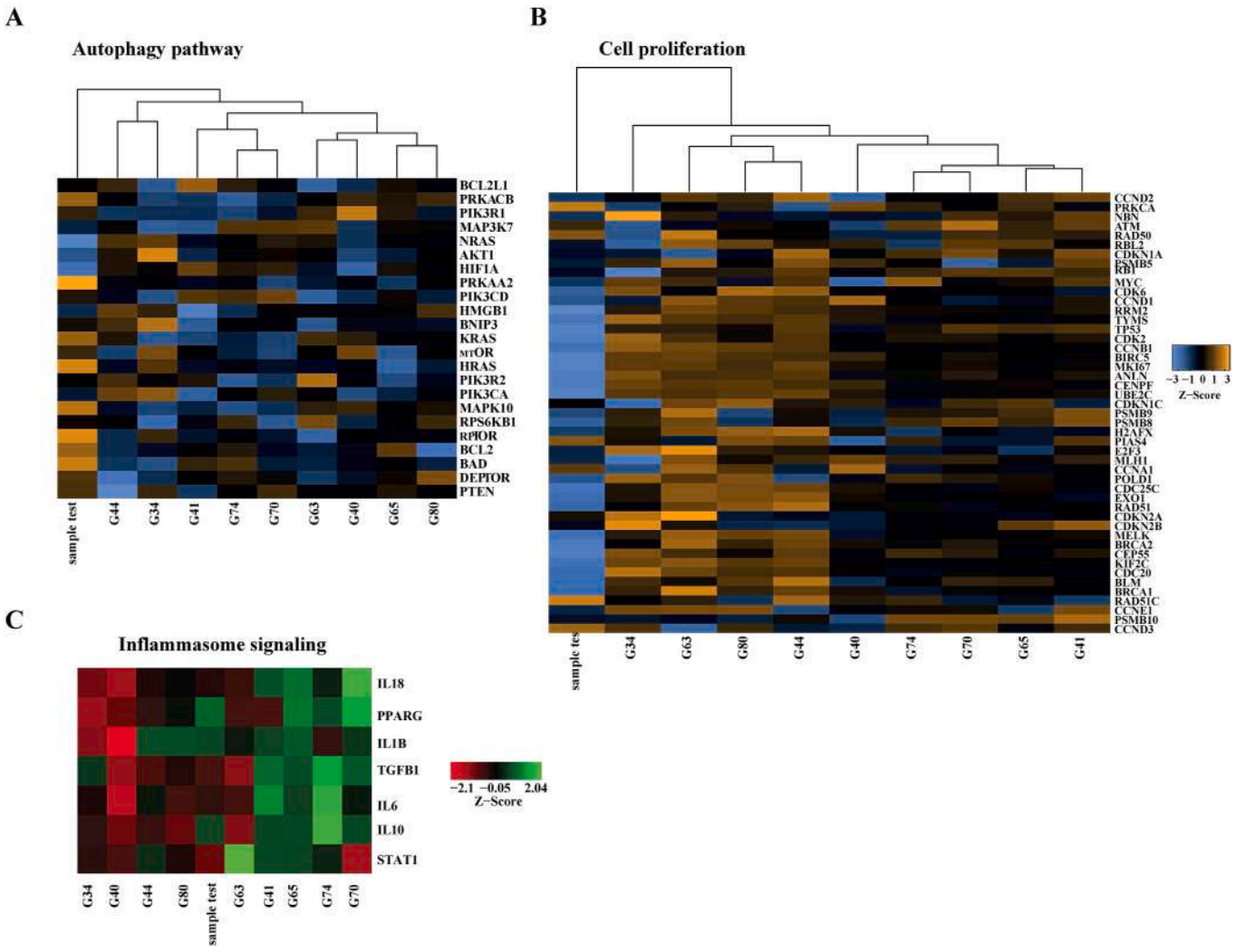

Fig. 8. Nanostring transcriptional profiling of a panel of GBM tissues. A-B) Heatmap of hierarchical clustering of 10 samples extracted from GBM tissues (one test patient treated with HBO-RT, one recurrent [from which G34 cell lines were isolated] and 8 naïve GBM [from which G40 and G44 were isolated]) analysis of expression signatures. Each row represents a gene, and each column, a sample. A pseudo-colored representation of z-scored log2 ratio is shown. Yellow and blue colors indicate the level of up- and downregulation, respectively. **C)** Heatmap of Inflammasome signaling gene expression of 10 samples extracted from GBM tissues (one test patient treated with HBO-RT, one recurrent [from which G34 cell lines were isolated] and 8 naïve GBM [from which G40 and G44 were isolated]). Each row represents a gene, and each column, a sample. A pseudo-colored representation of z-scored log2 ratio is shown. Green and red colors indicate the level of up- and downregulation, respectively.

Bartolini: Resources. **Antonella Naldini:** Supervision.

All authors read and approved the manuscript for publication.

Funding

This research did not receive any specific grant from funding agencies in the public, commercial, or not-for-profit sectors.

Declaration of competing interest

The authors declare that they have no known competing financial interests or personal relationships that could have appeared to influence the work reported in this paper.

Acknowledgements

The authors thank Gráinne Tierney for editorial assistance.

Appendix A. Supplementary data

Supplementary data to this article can be found online at https://doi.org/10.1016/j.canlet.2021.02.019.

References

[1] M. Paolillo, C. Boselli, S. Schinelli, Glioblastoma under siege: an overview of current therapeutic strategies, Brain Sci. 8 (2018), https://doi.org/10.3390/brainsci8010015.

[2] R. Stupp, W.P. Mason, M.J. van den Bent, M. Weller, B. Fisher, M.J.B. Taphoorn, K. Belanger, A.A. Brandes, C. Marosi, U. Bogdahn, J. Curschmann, R.C. Janzer, S. K. Ludwin, T. Gorlia, A. Allgeier, D. Lacombe, J.G. Cairncross, E. Eisenhauer, R. O. Mirimanoff, Radiotherapy plus concomitant and adjuvant temozolomide for glioblastoma, N. Engl. J. Med. 352 (2005) 987–996, https://doi.org/10.1056/NEJMoa043330.

[3] R. Stupp, M.E. Hegi, W.P. Mason, M.J. van den Bent, M.J. Taphoorn, R.C. Janzer, S. K. Ludwin, A. Allgeier, B. Fisher, K. Belanger, P. Hau, A.A. Brandes, J. Gijtenbeek, C. Marosi, C.J. Vecht, K. Mokhtari, P. Wesseling, S. Villa, E. Eisenhauer, T. Gorlia, M. Weller, D. Lacombe, J.G. Cairncross, R.O. Mirimanoff, Effects of radiotherapy with concomitant and adjuvant temozolomide versus radiotherapy alone on survival in glioblastoma in a randomised phase III study: 5-year analysis of the EORTC-NCIC trial, Lancet Oncol. 10 (2009) 459–466, https://doi.org/10.1016/S1470-2045(09)70025-7.

[4] J.D. Bernstock, J.H. Mooney, A. Ilyas, G. Chagoya, D. Estevez-Ordonez, A. Ibrahim, I. Nakano, Molecular and cellular intratumoral heterogeneity in primary glioblastoma: clinical and translational implications, J. Neurosurg. (2019) 1–9, https://doi.org/10.3171/2019.5.jns19364.
[5] M.E. Davis, Glioblastoma: overview of disease and treatment, Clin. J. Oncol. Nurs. 20 (2016) 1–8, https://doi.org/10.1188/16.CJON.S1.2-8.
[6] D. Hambardzumyan, M. Squatrito, E. Carbajal, E.C. Holland, Glioma formation, cancer stem cells, and Akt signaling, Stem Cell Rev. 4 (2008) 203–210, https://doi.org/10.1007/s12015-008-9021-5.
[7] A. Martínez-González, G.F. Calvo, L.A. Pérez Romasanta, V.M. Pérez-García, Hypoxic cell waves around necrotic cores in glioblastoma: a biomathematical model and its therapeutic implications, Bull. Math. Biol. 74 (2012) 2875–2896, https://doi.org/10.1007/s11538-012-9786-1.
[8] Z. Li, S. Bao, Q. Wu, H. Wang, C. Eyler, S. Sathornsumetee, Q. Shi, Y. Cao, J. Lathia, R.E. McLendon, A.B. Hjelmeland, J.N. Rich, Hypoxia-inducible factors regulate tumorigenic capacity of glioma stem cells, Canc. Cell 15 (2009) 501–513, https://doi.org/10.1016/j.ccr.2009.03.018.
[9] C.T. Taylor, S.P. Colgan, Regulation of immunity and inflammation by hypoxia in immunological niches, Nat. Rev. Immunol. 17 (2017) 774–785, https://doi.org/10.1038/nri.2017.103.
[10] C.T. Taylor, G. Doherty, P.G. Fallon, E.P. Cummins, Hypoxia-dependent regulation of inflammatory pathways in immune cells, J. Clin. Invest. 126 (2016) 3716–3724, https://doi.org/10.1172/JCI84433.
[11] N. Colwell, M. Larion, A.J. Giles, A.N. Seldomridge, S. Sizdahkhani, M.R. Gilbert, D.M. Park, Hypoxia in the glioblastoma microenvironment: shaping the phenotype of cancer stem-like cells, Neuro Oncol. 19 (2017) 887–896, https://doi.org/10.1093/neuonc/now258.
[12] C. Lewis, C. Murdoch, Macrophage responses to hypoxia: implications for tumor progression and anti-cancer therapies, Am. J. Pathol. 167 (2005) 627–635, https://doi.org/10.1016/S0002-9440(10)62038-X.
[13] D. Laoui, E. Van Overmeire, G. Di Conza, C. Aldeni, J. Keirsse, Y. Morias, K. Movahedi, I. Houbracken, E. Schouppe, Y. Elkrim, O. Karroum, B. Jordan, P. Carmeliet, C. Gysemans, P. DeBaetselier, M. Mazzone, J.A. Van Ginderachter, Tumor hypoxia does not drive differentiation of tumor-associated macrophages but rather fine-tunes the M2-like macrophage population, Canc. Res. 74 (2014) 24–30, https://doi.org/10.1158/0008-5472.CAN-13-1196.
[14] N.A. Charles, E.C. Holland, R. Gilbertson, R. Glass, H. Kettenmann, The brain tumor microenvironment, Glia 60 (2012) 502–514, https://doi.org/10.1002/glia.21264.
[15] Z. Chen, D. Hambardzumyan, Immune microenvironment in glioblastoma subtypes, Front. Immunol. 9 (2018) 1–8, https://doi.org/10.3389/fimmu.2018.01004.
[16] N. Wang, H. Liang, K. Zen, Molecular mechanisms that influence the macrophage M1-M2 polarization balance, Front. Immunol. 5 (2014), https://doi.org/10.3389/fimmu.2014.00614.
[17] D. Singh, R. Arora, P. Kaur, B. Singh, R. Mannan, S. Arora, Overexpression of hypoxia-inducible factor and metabolic pathways: possible targets of cancer, Cell Biosci. 7 (2017) 1–9, https://doi.org/10.1186/s13578-017-0190-2.
[18] A. Monteiro, R. Hill, G. Pilkington, P. Madureira, The role of hypoxia in glioblastoma invasion, Cells 6 (2017) 45, https://doi.org/10.3390/cells6040045.
[19] F. Hirschhaeuser, U.G.A. Sattler, W. Mueller-Klieser, Lactate: a metabolic key player in cancer, Canc. Res. 71 (2011) 6921–6925, https://doi.org/10.1158/0008-5472.CAN-11-1457.
[20] P.M. Tibbles, J.S. Edelsberg, Hyperbaric-oxygen therapy, N. Engl. J. Med. 334 (1996) 1642–1648, https://doi.org/10.1056/NEJM199606203342506.
[21] K. Stępień, R.P. Ostrowski, E. Matyja, Hyperbaric oxygen as an adjunctive therapy in treatment of malignancies, including brain tumours, Med. Oncol. 33 (2016) 1–9, https://doi.org/10.1007/s12032-016-0814-0.
[22] S.M. Hatfield, J. Kjaergaard, D. Lukashev, T.H. Schreiber, B. Belikoff, R. Abbott, S. Sethumadhavan, P. Philbrook, K. Ko, R. Cannici, M. Thayer, S. Rodig, J.L. Kutok, E.K. Jackson, B. Karger, E.R. Podack, A. Ohta, M.V. Sitkovsky, Immunological mechanisms of the antitumor effects of supplemental oxygenation, Sci. Transl. Med. 7 (2015), https://doi.org/10.1126/scitranslmed.aaa1260.
[23] J.R. Chen, H.Z. Xu, J.B. Ding, Z.Y. Qin, Radiotherapy after hyperbaric oxygenation in malignant gliomas, Curr. Med. Res. Opin. 31 (2015), https://doi.org/10.1185/03007995.2015.1082988, 1977–1984.
[24] A. Tesei, A. Sarnelli, C. Arienti, E. Menghi, L. Medri, E. Gabucci, S. Pignatta, M. Falconi, R. Silvestrini, W. Zoli, V. D'Errico, A. Romeo, E. Parisi, R. Polico, In vitro irradiation system for radiobiological experiments, Radiat. Oncol. 8 (2013) 257, https://doi.org/10.1186/1748-717X-8-257.
[25] S. Borowicz, M. Van Scoyk, S. Avasarala, M.K. Karuppusamy Rathinam, J. Tauler, R.K. Bikkavilli, R.A. Winn, The soft agar colony formation assay, JoVE (2014), https://doi.org/10.3791/51998.
[26] O. Garcia, I. Romero, J.E. González, T. Mandina, Measurements of DNA damage on silver stained comets using free Internet software, Mutat. Res. Toxicol. Environ. Mutagen. 627 (2007) 186–190, https://doi.org/10.1016/j.mrgentox.2006.11.007.
[27] S. Pignatta, M. Cortesi, C. Arienti, M. Zanoni, C. Cocchi, A. Sarnelli, D. Arpa, F. Piccinini, A. Tesei, Effects of Radiotherapy and Short-Term Starvation Combination on Metastatic and Non-tumor Cell Lines, DNA Repair (Amst), 2020, p. 102949, https://doi.org/10.1016/j.dnarep.2020.102949.
[28] J. Shah, Hyperbaric oxygen therapy, J. Am. Col. Certif. Wound Spec. 2 (2010) 9–13, https://doi.org/10.1016/j.jcws.2010.04.001.
[29] I. Marchiq, J. Pouysségur, Hypoxia, cancer metabolism and the therapeutic benefit of targeting lactate/H+ symporters, J. Mol. Med. 94 (2016) 155–171, https://doi.org/10.1007/s00109-015-1307-x.
[30] L.E.B. Stuhr, A. Raa, A.M. Øyan, K.H. Kalland, P.O. Sakariassen, K. Petersen, R. Bjerkvig, R.K. Reed, Hyperoxia retards growth and induces apoptosis, changes in vascular density and gene expression in transplanted gliomas in nude rats, J. Neuro Oncol. 85 (2007) 191–202, https://doi.org/10.1007/s11060-007-9407-2.
[31] Y.G. Wang, Y.P. Zhan, S.Y. Pan, H.D. Wang, D.X. Zhang, K. Gao, X.L. Qi, C.J. Yu, Hyperbaric oxygen promotes malignant glioma cell growth and inhibits cell apoptosis, Oncol. Lett. 10 (2015) 189–195, https://doi.org/10.3892/ol.2015.3244.
[32] C.H. Chang, Hyperbaric oxygen and radiation therapy in the management of glioblastoma, Natl. Cancer Inst. Monogr. 46 (1977) 163–169. http://europepmc.org/article/med/206835. (Accessed 11 August 2020). accessed.
[33] The Therapeutic Effect of Photon Irradiation on Viable Glioblastoma Cells Is Reinforced by Hyperbaric Oxygen | Request PDF, n.d, accessed, https://www.researchgate.net/publication/274781359_The_Therapeutic_Effect_of_Photon_Irradiation_on_Viable_Glioblastoma_Cells_Is_Reinforced_by_Hyperbaric_Oxygen. (Accessed 11 August 2020).
[34] L. Vande Walle, M. Lamkanfi, Pyroptosis, Curr. Biol. 26 (2016) R568–R572, https://doi.org/10.1016/j.cub.2016.02.019.
[35] D. Sharma, T.D. Kanneganti, The cell biology of inflammasomes: mechanisms of inflammasome activation and regulation, J. Cell Biol. 213 (2016) 617–629, https://doi.org/10.1083/jcb.201602089.
[36] J.M. Heddleston, M. Hitomi, M. Venere, W.A. Flavahan, K. Yang, Y. Kim, S. Minhas, J.N. Rich, A.B. Hjelmeland, Glioma stem cell maintenance: the role of the microenvironment, Curr. Pharmaceut. Des. 17 (2011) 2386–2401, https://doi.org/10.2174/138161211797249260.
[37] N. Charles, T. Ozawa, M. Squatrito, A.M. Bleau, C.W. Brennan, D. Hambardzumyan, E.C. Holland, Perivascular nitric oxide activates notch signaling and promotes stem-like character in PDGF-induced glioma cells, Cell Stem Cell 6 (2010) 141–152, https://doi.org/10.1016/j.stem.2010.01.001.
[38] O. Warburg, On the Origin of Cancer Cells, 1956.
[39] M.G. Vander Heiden, L.C. Cantley, C.B. Thompson, Understanding the Warburg effect: the metabolic requirements of cell proliferation NIH public access, Science 324 (2009) 1029–1033, https://doi.org/10.1126/science.1160809, 80.
[40] K.G. de la Cruz-López, L.J. Castro-Muñoz, D.O. Reyes-Hernández, A. García-Carrancá, J. Manzo-Merino, Lactate in the regulation of tumor microenvironment and therapeutic approaches, Front. Oncol. 9 (2019) 1143, https://doi.org/10.3389/fonc.2019.01143.
[41] M. Zanoni, S. Pignatta, C. Arienti, M. Bonafè, A. Tesei, Anticancer drug discovery using multicellular tumor spheroid models, Expet Opin. Drug Discov. 14 (2019) 289–301, https://doi.org/10.1080/17460441.2019.1570129.
[42] M. Zanoni, M. Cortesi, A. Zamagni, C. Arienti, S. Pignatta, A. Tesei, Modeling neoplastic disease with spheroids and organoids, J. Hematol. Oncol. 13 (2020), https://doi.org/10.1186/s13045-020-00931-0.
[43] D. Hambardzumyan, D.H. Gutmann, H. Kettenmann, The role of microglia and macrophages in glioma maintenance and progression, Nat. Neurosci. 19 (2015) 20–27, https://doi.org/10.1038/nn.4185.
[44] N. Kaminsky, O. Bihari, S. Kanner, A. Barzilai, Connecting malfunctioning glial cells and brain degenerative disorders, Dev. Reprod. Biol. 14 (2016) 155–165, https://doi.org/10.1016/j.gpb.2016.04.003.
[45] H. Qian, Q. Li, W. Shi, Hyperbaric oxygen alleviates the activation of NLRP-3-inflammasomes in traumatic brain injury, Mol. Med. Rep. 16 (2017) 3922–3928, https://doi.org/10.3892/mmr.2017.7079.
[46] S. Müller, G. Kohanbash, S.J. Liu, B. Alvarado, D. Carrera, A. Bhaduri, P. B. Watchmaker, G. Yagnik, E. Di Lullo, M. Malatesta, N.M. Amankulor, A. R. Kriegstein, D.A. Lim, M. Aghi, H. Okada, A. Diaz, Single-cell profiling of human gliomas reveals macrophage ontogeny as a basis for regional differences in macrophage activation in the tumor microenvironment, Genome Biol. 18 (2017), https://doi.org/10.1186/s13059-017-1362-4.
[47] S. Loeffler, B. Fayard, J. Weis, J. Weissenberger, Interleukin-6 induces transcriptional activation of vascular endothelial growth factor (VEGF) in astrocytes in vivo and regulates VEGF promoter activity in glioblastoma cells via direct interaction between STAT3 and Sp1, Int. J. Canc. 115 (2005) 202–213, https://doi.org/10.1002/ijc.20871.
[48] M. Orecchioni, Y. Ghosheh, A.B. Pramod, K. Ley, Macrophage polarization: different gene signatures in M1(Lps+) vs. Classically and M2(LPS-) vs. Alternatively activated macrophages, Front. Immunol. 10 (2019), https://doi.org/10.3389/fimmu.2019.01084.
[49] C. Moratal, J. Raffort, N. Arrighi, S. Rekima, S. Schaub, C.A. Dechesne, G. Chinetti, C. Dani, IL-1β- and IL-4-polarized macrophages have opposite effects on adipogenesis of intramuscular fibro-adipogenic progenitors in humans, Sci. Rep. 8 (2018), https://doi.org/10.1038/s41598-018-35429-w.